Raman Evidence for Meisenheimer Complex Formation in the Hydrolysis Reactions of 4-Fluorobenzoyl- and 4-Nitrobenzoyl-Coenzyme A Catalyzed by 4-Chlorobenzoyl-Coenzyme A Dehalogenase†

Jian Dong and Paul R. Carey*

Department of Biochemistry, Case Western Reserve University, Cleveland, Ohio 44106

Yansheng Wei, Lusong Luo, Xuefeng Lu, Rui-Qin Liu,‡ and Debra Dunaway-Mariano*

Department of Chemistry, University of New Mexico, Albuquerque, New Mexico 87131

Received March 5, 2002; Revised Manuscript Received April 16, 2002

ABSTRACT: 4-Chlorobenzoyl-coenzyme A (4-CBA-CoA) dehalogenase catalyzes the hydrolytic dehalogenation of 4-CBA-CoA to 4-hydroxybenzoyl-CoA by using an active site Asp145 carboxylate as the nucleophile. Formation of the corresponding Meisenheimer complex (EMc) is followed by chloride ion expulsion to form arylated enzyme (EAr). The EAr is then hydrolyzed to product. In this paper, we report the kinetics for dehalogenase-catalyzed 4-fluorobenzoyl-CoA (4-FBA-CoA) and 4-nitrobenzoyl-CoA (4-NBA-CoA) hydrolysis and provide Raman spectral evidence for the accumulation of EMc in these reactions. The 4-FBA-CoA and 4-NBA-CoA substrate analogues were selected for the poor leaving group ability of their C(4) substituents. Thus, the formation of the EAr from EMc should be hindered, giving rise to a quasi-steady-state equilibrium between EMc and the Michaelis complex. Detailed kinetic studies were carried out to quantitate the composition of the reaction mixtures. Quench experiments demonstrated that significant populations of EAr do not exist in reaction mixtures involving the 4-F- or 4-N-substrates. A kinetic model enabled us to estimate that approximately 10−20% of the enzyme−substrate complexes in the reaction mixtures are present as EMc. Raman difference spectra of 4-NBA-CoA and 4-FBA-CoA bound to WT and H90Q mutant dehalogenase have broad features near 1500 and 1220 cm^{-1} that are absent in the free ligand. Crucially, these features are also absent in the Raman spectra of the complexes involving the D145A dehalogenase mutant that are unable to form an EMc. Quantum mechanical calculations, at the DFT level, provide strong support for assigning the novel 1500 and 1220 cm^{-1} features to an EMc.

4-Chlorobenzoyl-coenzyme A (4-CBA-CoA)[1] dehalogenase (*1*−*3*) mediates the central reaction of the 4-chlorobenzoate (4-CBA) to 4-hydroxybenzoate (4-HBA) pathway found in certain soil-dwelling bacteria (*4*). Previous studies of substrate activation and turnover occurring within the dehalogenase active site have revealed an elaborate catalytic mechanism (*5*−*15*). The individual steps proposed for the reaction are illustrated in Figure 1. According to this mechanism, substrate binding to the dehalogenase active site is followed by attack of the carboxylate side chain of Asp145 at the benzoyl C(4). The Meisenheimer complex formed (henceforth referred to as the EMc intermediate) ultimately expels the Cl^- ion, thus forming an arylated enzyme complex (the EAr intermediate). Hydrolysis of the ester function in EAr then occurs, forming the 4-HBA-CoA product, which along with a proton and the Cl^- ion is released from the enzyme active site.

The first step of catalysis, substrate activation through thioester C═O polarization, is achieved via H-bonds formed to two active site backbone amide N−Hs, one of which (Gly114) is positioned at the positive pole of an α-helix dipole and the other of which (Phe64) is coupled to the binding of the CoA moiety [backbone C═O to Ade C(6)-NH_2] (see active site pictured in Figure 2) (*6*). The electron "pull" provided to the C═O is augmented by an electron "push" from the carboxylate of Asp145 poised at C(4) of the substrate benzoyl ring (*7*−*9*). The electrostatic interactions are facilitated by the sheath of aromatic side chains (Phe64, Phe82, Trp137, and Trp89) encircling the benzoyl

† This research was supported by NIH Grants GM-28688 (to D.D.-M.) and GM-54072 (to P.R.C.).

* To whom correspondence should be addressed. P.R.C.: phone 216-368-0031, fax 216-368-3419, e-mail carey@biochemistry.cwru.edu. D.D.-M.: phone 505-277-3383, fax 505-277-6202, e-mail dd39@unm.edu.

‡ Current address: Dupont Pharmaceutical Co., Hockessin, DE 29707.

[1] Abbreviations: 4-CBA, 4-chlorobenzoate; 4-CBA-CoA, 4-chlorobenzoyl-coenzyme A; 4-HBA-CoA, 4-hydroxybenzoyl-CoA; 4-FBA-CoA, 4-fluorobenzoyl-CoA; 4-NBA-CoA, 4-nitrobenzoyl-CoA; Hepes, *N*-(2-hydroxyethyl)piperazine-*N*′-2-ethanesulfonic acid; Tris, tris(hydroxymethyl)aminomethane; WT, wild-type; E·S, dehalogenase−4-XBA-CoA complex in which X = chloro, fluoro, or nitro; E·P, dehalogenase−4-HBA-CoA complex; EMc, Meisenheimer complex (ó-complex) formed by addition of the dehalogenase Asp145 to the substrate benzoyl C(4); EAr, benzoyl-CoA ester formed with the dehalogenase active site Asp145; S_NAr, aromatic nucleophilic substitution; H-bond, hydrogen bond; HPLC, high-performance liquid chromatography; DFT, density functional theory; HF, Hartree−Fock.

10.1021/bi020186+ CCC: $22.00
Published on Web 05/17/2002

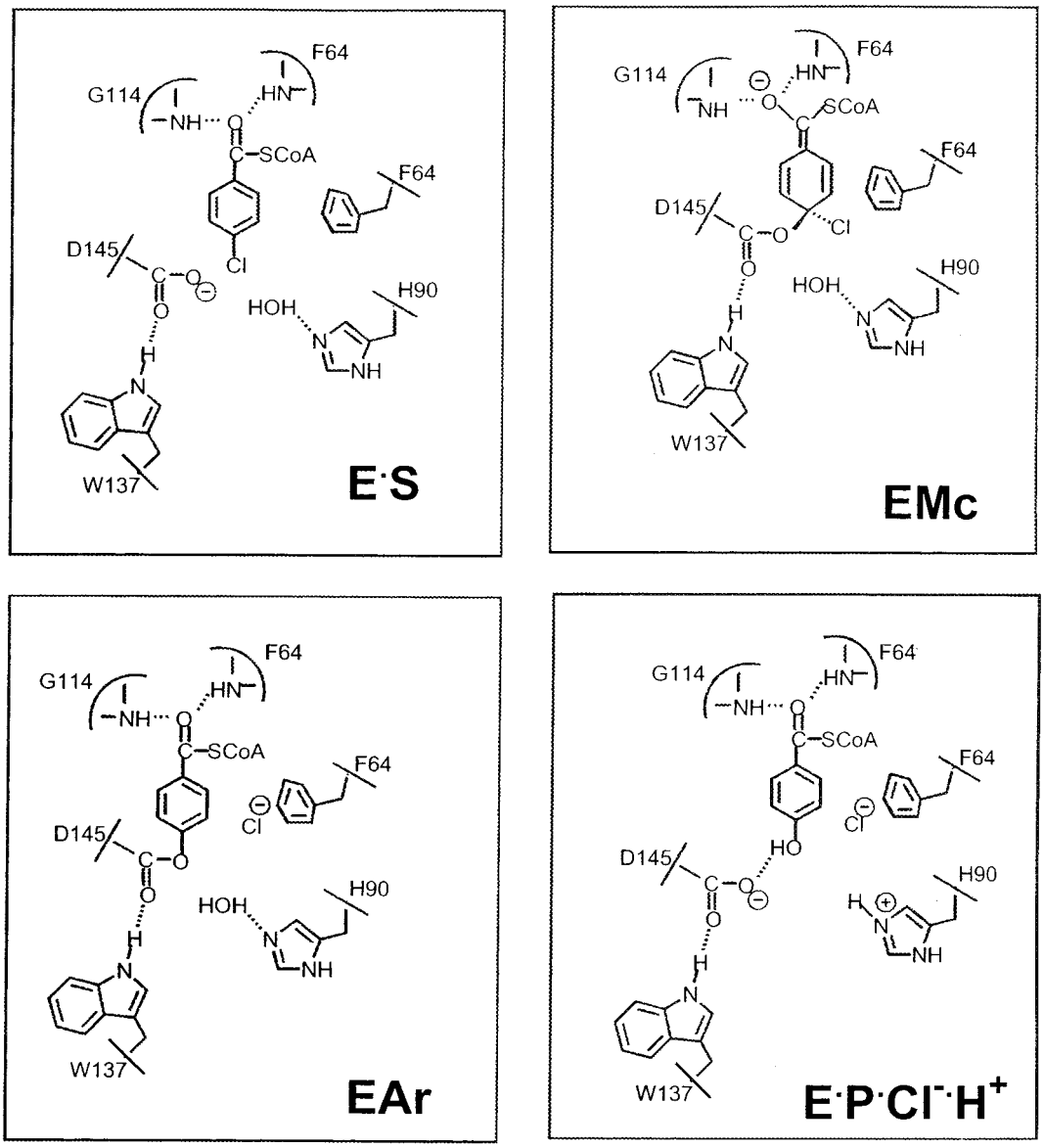

FIGURE 1: Proposed chemical steps of the *Pseudomonas sp.* strain CBS-3 4-CBA-CoA dehalogenase-catalyzed conversion of 4-CBA-CoA to 4-HBA-CoA.

moiety. The overall effect of the active site environment on the substrate is dispersion of the ring π electron density away from C(4) and toward the thioester C═O.

The ensuing attack made by the Asp145 at the C(4) of the polarized benzoyl ring has been evidenced through several independent lines of experimental investigation. First, from the X-ray structure of the 4-CBA-CoA dehalogenase−4-HBA-CoA complex (*10*), the Asp145 carboxylate oxygen Oδ2 is seen positioned in an "attack conformation" (*16, 17*), 2.5 Å from C(4) (see Figure 2). Second, within the detection limit of the rate measurement ($\sim 1 \times 10^{-7}$ s^{-1}), the D145A mutant has been found to be "catalytically inactive" (*18*). Third, it has been shown that single-turnover reactions carried out in oxygen-18-enriched water produce [C(4)-^{16}O]4-HBA-CoA as product [i.e., the C(4)OH is derived from an active site carboxylate] (*13, 14*). Finally, single-turnover reactions carried out with [^{14}C]4-CBA-CoA in conjunction with rapid quench techniques have demonstrated the formation and decay of a kinetically competent covalent enzyme intermediate (*5, 14*). These data are consistent with a reaction mechanism that involves the arylation of Asp145 and subsequent hydrolysis of the aryl ester at the Asp145 C═O. The close proximity (2.9 Å) of the Trp137 indole NH to the Asp145 Oδ1 (Figure 1) indicates that it functions to orient the carboxylate nucleophile and/or activate the Asp145 aryl ester (Figure 2). Likewise, the positioning of the His90 N(3) at 3.6 Å from the Asp145 carboxyl carbon suggests its participation in binding and activating the water nucleophile involved in the hydrolysis of the EAr intermediate. Results from a kinetic analysis of the H90Q mutant support the role of His90 in general base catalysis in EAr hydrolysis (*5*).

The formation of Meisenheimer complex intermediates in the nucleophilic substitution reactions of electrophilic aromatic rings is well documented (*19, 20*). Nitro substituents are especially effective in activating the ring for nucleophilic attack because they provide resonance stabilization to the anionic σ-complex. The UV/visible absorption spectra of the Meisenheimer intermediates formed from the reaction of nitro-substituted aromatic rings are strongly red-shifted, thus allowing easy detection of the intermediate. A most striking

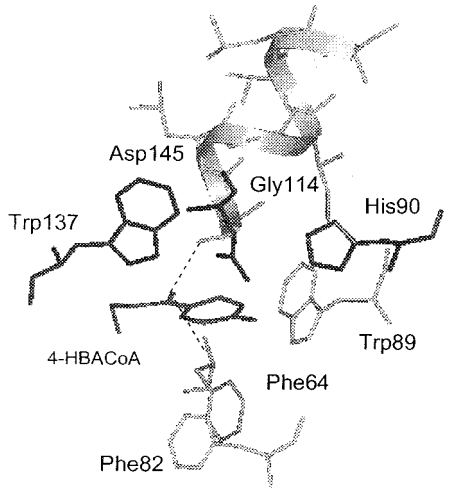

FIGURE 2: Active site region of the *Pseudomonas sp*. strain CBS-3 4-CBA-CoA dehalogenase−4-HBA-CoA complex generated using the X-ray crystallographic structural coordinates reported in ref (*10*) and Insight II. The 4-hydroxybenzoyl-CoA ligand is truncated to show only the hydroxybenzoyl end.

example of biological Meisenheimer complex formation is seen with the development of an orange−red color in culture media containing *Rhodococcus erythropolis* and 2,4,6-trinitrobenzene (*21*). Studies have shown that this color is derived from hydride transfer to the aromatic ring to form the anionic σ-complex (*22*). Because hydride and nitrite are poor leaving groups, the Meisenheimer complex persists.

Glutathione transferase-catalyzed nucleophilic aromatic substitution reactions have been well characterized. Glutathione transferase catalyzes the formation of the thiolate anion of glutathione and its addition to a variety of carbon electrophiles, including highly activated aromatic rings. The addition of glutathione to activated aromatic rings having poor leaving groups produces relatively stable Meisenheimer complexes (the glutathione anion is also a poor leaving group) which are further stabilized through tight binding by the enzyme active site (*23*, *24*). The X-ray crystal structures of the class μ (*25*) and class π (*26*) glutathione transferases bound with 1-(*S*-glutathionyl)-2,4,6-trinitrocyclohexadienate anion have been reported, and these structures reveal stabilization through H-bond interactions occurring between the nitro substituents and the enzyme active site.

The aromatic substitution reaction catalyzed by the 4-CBA-CoA dehalogenase differs from that catalyzed by the glutathione transferase in two important ways. First, the aromatic ring of the substrate is only weakly electrophilic, and therefore it must be fully activated for nucleophilic attack by the enzyme active site. The EMc, which is formed at an estimated rate of 200 s^{-1} (see kinetic mechanism illustrated in Figure 3), is stabilized through a network of H-bonding groups originating at the thioester C═O (Figure 1) (*6*, *27*). Second, in the dehalogenase, the nucleophile is the carboxylate Asp145 and not a thiolate anion. Unlike the thiolate anion, the carboxylate is an excellent leaving group. Consequently, the reversion of the EMc to E·S is competitive with its partitioning forward to EAr. Kinetic studies have indicated that the EMc expels the carboxylate residue at an estimated rate of 2000 s^{-1} while it expels the chloride ion at a rate of 40 s^{-1} (*5*). The EMc intermediate does not accumulate to a significant extent during substrate turnover

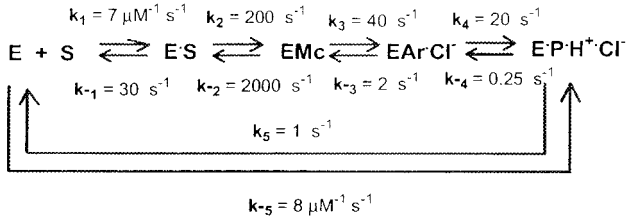

FIGURE 3: Kinetic model for *Pseudomonas sp*. strain CBS-3 4-chlorobenzoyl-CoA dehalogenase catalysis adapted from ref (*5*). E is the dehalogenase, S is 4-chlorobenzoyl-CoA, EMc is the Meisenheimer intermediate, EAr is the arylated enzyme intermediate, and P is 4-hydroxybenzoyl-CoA.

and is therefore difficult to observe. Through the use of an alternate substrate in which the chloride substituent is replaced by a leaving group having less mobility (fluoride or nitrite), the rate at which the EMc partitions forward can be significantly reduced. This will allow an equilibrium to be established between the E·S and EMc complexes, governed by the relative rates of Asp145 addition to substrate and expulsion from EMc. Based on these rates, we anticipated that ca. 10−20% of the dehalogenase may be populated as the EMc. Raman spectroscopic data, supported strongly by quantum mechanical calculations, provide good evidence that a population of EMcs does indeed exist in reaction mixtures containing the 4-NBA-CoA or 4-FBA-CoA analogues.

EXPERIMENTAL PROCEDURES

General. 4-CBA-CoA, 4-FBA-CoA, and 4-HBA-CoA were prepared according to ref (*15*). 4-NBA-CoA was synthesized from coenzyme A and 4-nitrobenzoyl chloride by adaptation of the procedure described in ref (*28*). 4-CBA-CoA dehalogenase (specific activity = 1.5 units/mg) and the D145A, H90Q mutants were prepared according to the published procedure (*14*). Enzyme concentration was determined by using the Bradford method (*29*).

Ligand Dissociation Constants Measured by Fluorescence Quenching. A FluoroMax-2 fluorometer was used in protein fluorescence quenching experiments aimed at measuring the binding constants of 4-FBA-CoA and 4-HBA-CoA with 4-CBA-CoA dehalogenase. The fluorescence spectrum of dehalogenase (1 μM) in 50 mM K^+Hepes (pH 7.5, 25 °C) resulting from 290 nm excitation has an emission wavelength maximum at 337 nm. For a typical titration experiment, 1−10 μL aliquots of ligand were added to a 1 mL solution of 1 μM dehalogenase, and the fluorescence intensity at 337 nm was measured following each addition. The fluorescence data, collected at ligand concentrations ranging from 0.1 to 60 μM for 4-FBA-CoA and from 0.1 to 10 μM for 4-NBA-CoA, were fitted to eq 1 (*30*) using the Kaleida Graph computer program for nonlinear regression analysis:

$$\Delta F/F_0 = (\Delta F_{max}/F_0 \cdot [E])\{(K_d + [E] + [S]) - \sqrt{(K_d + [E] + [S])^2 - 4[E][S]}\}/2 \quad (1)$$

where [S] is the total ligand concentration, [E] is the total enzyme concentration, K_d is the apparent dissociation constant of the enzyme−ligand complex, ΔF is the observed change in fluorescence intensity, ΔF_{max} is the maximum change in fluorescence intensity, and F_0 is the initial fluorescence intensity.

Ligand Binding Rates Measured by Stopped-Flow Fluorescence. For fluorescence kinetic measurements, a DX.17 MV stopped-flow spectrometer (Applied Photophysics, Leatherhead, U.K.) equipped with a 150 W xenon lamp (2 mm slit width) was used. The excitation wavelength was 290 nm, and the emission filter cutoff was 320 nm. Data acquisition and processing was controlled by a 32-bit processor Archimedes workstation, which was also used for subsequent nonlinear regression analysis of the kinetic traces. Stock solutions of ligand and enzyme were diluted to specific concentrations with 50 mM K^+Hepes buffer (pH 7.5, 25 °C). Data sets were collected in triplicate and averaged. The fluorescence quenching traces were analyzed with a single-exponential equation to obtain the observed rate constant, k_{obs}. The plot of k_{obs} vs ligand concentration was linear for each reaction. These data were fit to eq 2 to obtain k_{on} and k_{off}.

$$k_{obs} = k_{off} + k_{on}[S] \quad (2)$$

In eq 2, [S] = substrate concentration, k_{obs} = observed rate constant, k_{on} = binding rate constant, and k_{off} = dissociation rate constant.

Reaction Progress Curves Measured by 4-HBA-CoA Spectrophotometric Detection. (A) Multiple Turnover Reactions. Reaction solutions initially contained 20 μM 4-CBA-CoA dehalogenase and 200 μM 4-NBA-CoA in 50 mM K^+Hepes (pH 7.5, 25 °C) or contained 44.5 μM 4-CBA-CoA dehalogenase and 300 μM 4-FBA-CoA in 50 mM K^+-Hepes (pH 7.5, 25 °C). After a specified incubation period, a 110 μL aliquot was removed from the 4-NBA-CoA reaction mixture and mixed with 110 μL of 0.3 M KOH. The absorbance of the resulting solution was measured at 330 nm (ϵ = 18.2 mM^{-1} cm^{-1} for the 4-HBA-CoA phenoxide anion). In the case of the 4-FBA-CoA reaction, 25 μL of 2.5 M KOH was added directly to the reaction solution, and the absorbance at 330 nm was measured.

(B) Single-Turnover Reactions. The reaction between 30 μL of 250 μM 4-CBA-CoA dehalogenase in 50 mM K^+-Hepes (pH 7.5, 25 °C) and 32 μL of 201 μM 4-CBA-CoA in 50 mM K^+Hepes (pH 7.5, 25 °C) was carried out in a KINTEK rapid quench device. After a specified incubation period, the reaction was quenched with 182 μL of 0.32 M HCl. Then 40 μL of (saturated) 4 M KCl was added to facilitate enzyme precipitation. The mixture was centrifuged in a 0.5 mL NANOSEP MF 0.2 μm centrifugal device (Pall Filtron Corp.). A 220 μL aliquot of the supernatant fraction was mixed with 34 μL of 2.5 M KOH, and the absorbance of the resulting solution at 330 nm was measured. The enzyme precipitant contained in the centrifugal device was suspended in a 250 μL solution containing 0.2 M HCl and 0.56 M KCl and then centrifuged. This cycle was repeated twice more. The washed enzyme precipitant was then dissolved in 230 μL of 0.15 M KOH and centrifuged, and the absorbance of the resulting solution at 330 nm was measured. The reaction between the dehalogenase and 4-NBA-CoA was not carried out in the rapid quench device. Instead, after a specified incubation period, the 250 μL reaction solution initially containing 70 μM dehalogenase and 60 μM 4-NBA-CoA in 50 mM K^+Hepes (pH 7.5, 25 °C) was hand-mixed with 10 μL of 6 M HCl and 40 μL of 4 M KCl. The reaction mixture was separated and analyzed as previously described.

UV/Visible Difference Spectra, Stopped-Flow Absorption Measurements, and Data Analyses. UV/visible difference spectra were measured as described in Taylor et al. (*9*). The absorption reference spectra were measured by using 1 mL quartz tandem cells containing 0.5 mL of enzyme solution in one compartment and 0.5 mL of 4-FBA-CoA or 4-NBA-CoA solution in the other. All solutions were buffered with 50 mM K^+Hepes (pH 7.5, 1 mM DTT, 25 °C). The reference absorbance spectrum was recorded and subtracted from the spectrum of the mixed solutions to give the difference spectra of the enzyme−4-FBA-CoA or −4-NBA-CoA complex. For UV/visible absorption kinetic measurements, a DX.17 MV stopped-flow spectrometer (Applied Photophysics, Leatherhead, U.K.) equipped with a 150 W xenon lamp (1 mm slit width, 1 cm path length) was used. Stock solutions of ligand and enzyme were diluted to specific concentrations with 50 mM K^+Hepes buffer (pH 7.5, 25 °C). Reactions were monitored at 430 and 375 nm over 0−200 ms and 0−3600 s time periods. Data sets were collected in triplicate and averaged. The computer program KINSIM (*31*) was used to simulate curves to the absorption traces using the microscopic rate constants and molar extinction coefficients of the absorbing species as input.

Raman Spectroscopy. The nonresonant Raman spectra were obtained using 647.1 nm laser excitation from an Innova 400 krypton laser system (Coherent, Inc.), a back-illuminated charge-coupled device (CCD) detector (model 1024EHRB/1, Princeton Instruments, Inc.) operating at 183 K, and a Holospec f/1.4 axial transmission spectrometer (Kaiser Optical Systems, Inc.) employed as a single monochromator, as described in a previous report (*7*). Enzyme samples contained in cuvettes were 50 μL in volume and buffered with 50 mM Tris-HCl at pH 7.5. Enzyme and 4-FBA-CoA or 4-NBA-CoA concentrations used are given in the figure legends. Data were collected immediately after the complex had been made, using a laser power of ~850 mW and CCD exposure times of 5 min. The Raman spectrum of the buffer was subtracted from that of the ligand in buffer (giving the spectrum of free ligand), while the spectrum of the enzyme in buffer was subtracted from that of the enzyme−ligand complex to give the spectrum of the bound ligand.

Calculations. Quantum mechanical computations have been performed to determine the vibrational assignments of the Meisenheimer compounds (Mc) formed by the 4-N and 4-F analogues (Figure 8), and to provide insights into geometry changes occurring in the Mc. For the calculations, the bulky coenzyme A part was truncated to an *S*-ethyl, and the torsional angle about S−C was set at gauche [which is the same as the conformer found in the X-ray crystal data of the final product 4-HBA-CoA (*10*)]. The Asp145 side chain was represented by an acetate species (CH_3COO^-). 4-NBA-CoA and 4-FBA-CoA were also analyzed by substituting *S*-ethyl for the CoA, to confirm the ring modes of the benzoyl moiety, and the vibrational modes associated with the NO_2 and F substituents.

Using Gaussian 98 software (*32*), full geometry optimization of the molecules was carried out for the subsequent estimation of harmonic force constants at the density functional theory (DFT) level of B3LYP/6-31+G(d) [i.e., electron correlation effect included Becke's three-parameter exchange functional using the correlation functional of Lee, Yang, and Parr (*33, 34*)]. The same Gaussian basis set of

Table 1: Thermodynamic and Kinetic Constants Measured for 4-CBA-CoA Dehalogenase with 4-CBA-CoA, 4-FBA-CoA, and 4-NBA-CoA (Values Are Defined within 10% Error)

ligand	k_{on} (μM^{-1} s^{-1})	k_{off} (s^{-1})	K_d (μM)[a]	k (s^{-1})[b]
4-CBA-CoA[c]	7	30	4	2.3
4-NBA-CoA	2.4	1.0	0.5 (0.4)	1×10^{-3}
4-FBA-CoA	1.4	23	16 (16)	7×10^{-6}

[a] The K_d value not in parentheses was calculated from the binding rate constants while the K_d value in parentheses was determined by titration using fluorescence titration quenching methods. [b] The k value was determined by fitting product formation curves for a single turnover measured at saturating ligand concentration. [c] Values taken from ref (*5*).

6-31+G(d) was used for compounds I and II (as anions), and for 4-FBA-CoA and 4-NBA-CoA. The absence of imaginary vibrational frequencies confirmed that the optimized geometries correspond to ground-state energy minima, not to saddle points.

RESULTS AND DISCUSSION

Kinetic Analysis of Dehalogenase-Catalyzed Hydrolysis of 4-FBA-CoA and 4-NBA-CoA

Prior to carrying out Raman spectroscopic studies of the dehalogenase complexes of 4-FBA-CoA and 4-NBA-CoA, it was necessary to measure binding constants for these complexes and the rate at which they undergo reaction. Also, because the Raman analysis may detect any intermediate present in reaction mixture, it was important to show that the arylated enzyme does not accumulate in these mixtures.

Binding. The k_{on} and k_{off} values for the binding of 4-FBA-CoA and 4-NBA-CoA to 4-CBA-CoA dehalogenase were measured using stopped-flow fluorescence quenching techniques. The values obtained are listed in Table 1 along with those reported previously for 4-CBA-CoA (*5*). Based on the k_{on} and k_{off} values for 4-FBA-CoA, a $K_d = 16$ μM is calculated. The K_d calculated for 4-NBA-CoA is 0.5 μM. The K_d values for 4-FBA-CoA and 4-NBA-CoA compare with the $K_d = 4$ μM calculated from the binding rate constants obtained for 4-CBA-CoA (*5*).

Owing to slow turnover of the 4-FBA-CoA and 4-NBA-CoA ligands, fluorescence titration curves could be determined. These titration curves reflect the equilibria between free ligand and the enzyme−ligand complex plus EMc. For 4-FBA-CoA, the apparent $K_d = 16$ μM, and for 4-NBA-CoA, the apparent $K_d = 0.4$ μM. These values agree with the K_d values calculated from the binding rate constants.

Time Courses for Product Formation. The time course for product formation was examined under multiple-turnover conditions in which the 4-CBA-CoA dehalogenase (20 μM) is reacted with a 10-fold excess of 4-NBA-CoA (200 μM). The reactions were terminated by adding sufficient KOH solution to raise the pH to 14. Under these conditions, the enzyme is inactive, and the 4-HBA-CoA product exists as the phenoxide anion, which is detected at 330 nm. Figure 4A shows the product formation curve for the first several turnovers of 4-NBA-CoA. The first turnover (corresponding to 20 μM 4-HBA-CoA) occurs at the same rate as subsequent turnovers, indicating that a step preceding product release is rate-limiting. The turnover rate derived from the time course is 1×10^{-3} s^{-1}.

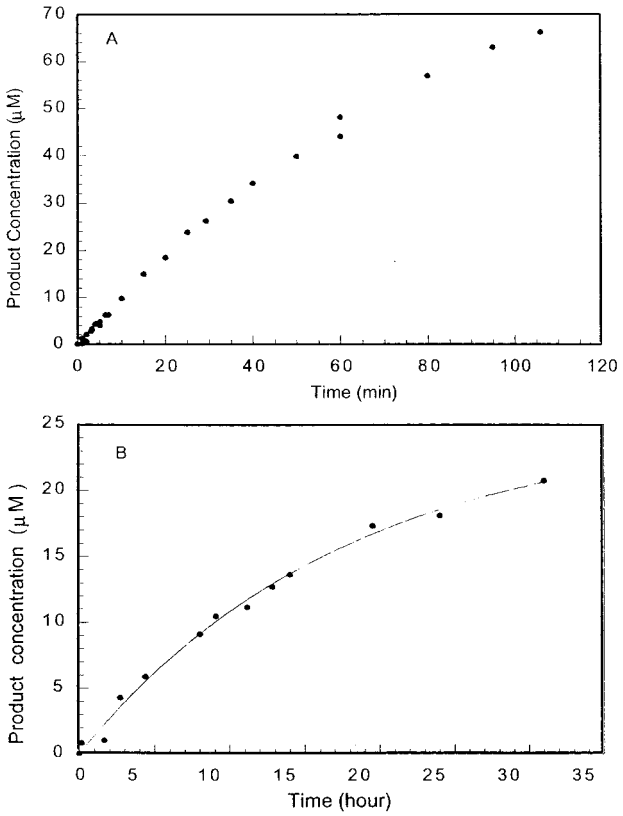

FIGURE 4: Time courses for the formation of 4-HBA-CoA in the reaction of (A) 200 μM 4-NBA-CoA and 20 μM wild-type 4-CBA-CoA dehalogenase in 50 mM K^+Hepes (pH 7.5, 25 °C) and (B) 300 μM 4-FBA-CoA and 44.5 μM wild-type 4-CBA-CoA dehalogenase in 50 mM K^+Hepes (pH 7.5, 25 °C).

The dehalogenase (44.5 μM)-catalyzed reaction of 4-FBA-CoA (300 μM) proved to be too slow to monitor over several turnovers. The time course shown in Figure 4B indicates that the enzyme completes only 50% of a turnover at 25 h. From the time course data, a turnover rate of 7×10^{-6} s^{-1} is obtained. The poor leaving ability ($F^- < NO_2^- < Cl^-$) in dehalogenase simply implies that breaking of the C4−X bond is rate-limiting in these alternative substrates, a phenomenon of S_NAr reactions that depends on the character of the nucleophile and the leaving group X− as well as the accessibility of a H-bond donor that may assist the departure of the X− (*20*, *35*).

A Probe for the Arylated Enzyme Intermediate. Previous studies have shown that during a single turnover of 4-CBA-CoA by the 4-CBA-CoA dehalogenase, both covalent enzyme intermediates accumulate on the enzyme (*5*). In contrast, we do expect to observe EAr accumulation during dehalogenase turnover of 4-FBA-CoA or 4-NBA-CoA. This is because once formed, the EMc will expel the fluoride or nitrite ion at a rate much slower than the anticipated rate of EAr hydrolysis. To test this hypothesis, we measured EAr accumulation during single-turnover reactions of 4-FBA-CoA and 4-NBA-CoA. To accomplish this, the original single-turnover experiment which employed [^{14}C]4-CBA-CoA (along with centrifugal molecular cutoff filtration of enzyme and HPLC separation of [^{14}C]4-CBA-CoA and [^{14}C]4-HBA-CoA) (*5*) was modified so that it could be carried out with unlabeled reactant.

The new EAr detection method was first demonstrated with 4-CBA-CoA serving as substrate. Reaction mixtures

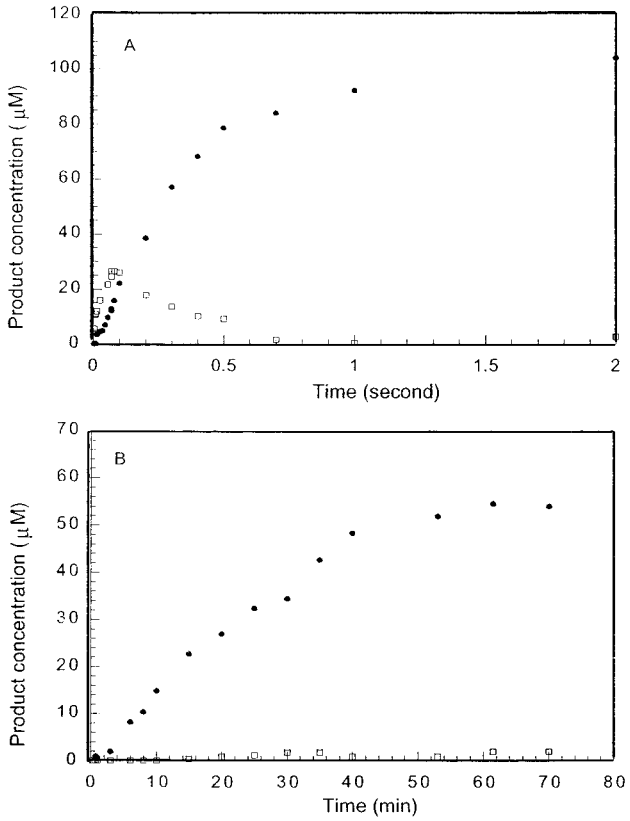

FIGURE 5: Time courses for the formation of EAr (denoted with open squares) and 4-HBA-CoA (denoted with solid circles) in the reaction of (A) 104 μM 4-CBA-CoA and 121 μM wild-type 4-CBA-CoA dehalogenase in 50 mM K^+Hepes (pH 7.5, 25 °C) and (B) 60 μM 4-NBA-CoA and 70 μM wild-type 4-CBA-CoA dehalogenase in 50 mM K^+Hepes (pH 7.5, 25 °C).

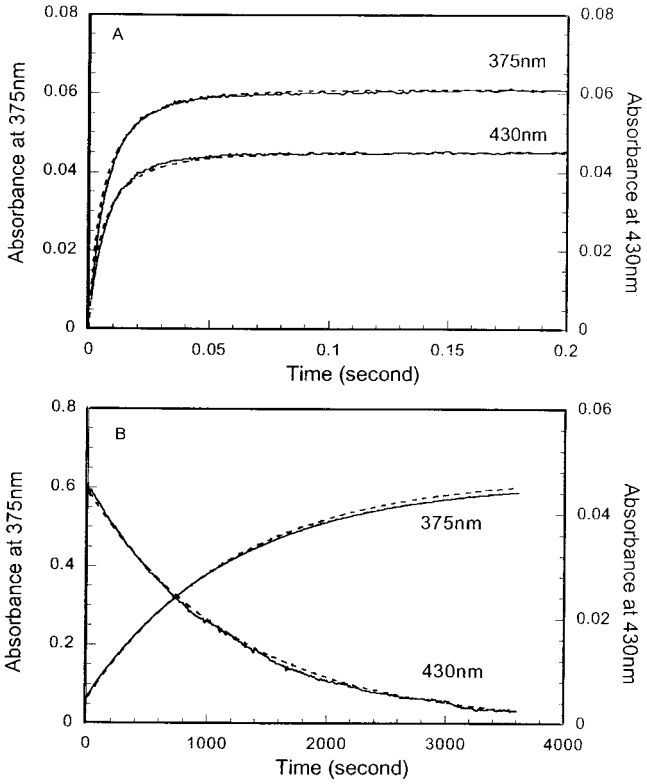

FIGURE 6: Stopped-flow absorption traces measured at 430 and 375 nm for reactions of 60 μM 4-NBA-CoA and 70 μM wild-type 4-CBA-CoA dehalogenase in 50 mM K^+Hepes (pH 7.5, 25 °C) over (A) a 0−200 ms time period and (B) a 0−3600 s time period.

of dehalogenase (121 μM) and 4-CBA-CoA (104 μM) were quenched with acid after specified incubation periods in a rapid quench device. The precipitated enzyme was separated, and the two fractions were treated with aqueous KOH to convert EAr (from enzyme precipitant) and 4-HBA-CoA (from the supernatant) to the phenoxide anion of the 4-HBA-CoA (detected at 330 nm). The time courses for EAr formation and product formation thus obtained are shown in Figure 5A. EMc present in the reaction solution at the time of the quench may also contribute to the EAr pool through expulsion of chloride ion. The time course reveals the accumulation of EAr over the first 100 ms to a level of 25% [isolation of labeled enzyme by precipitation proved to be more efficient than isolation by repetitive dilution and centrifugal molecular cutoff filtration of solvated enzyme as used previously to detect 16% accumulation; see ref (5)] and then a decline over the next 500 ms to 0%.

The same experiment was carried out with 4-NBA-CoA and 4-FBA-CoA, but owing to the slower reaction rate, the reactions were terminated by hand rather than by rapid quench. Only EAr will be detected in the quenched mixtures because EMc will expel the enzyme carboxylate more efficiently than the fluoride or nitrite ion. In Figure 5B, the time courses for EAr and product formation during the single-turnover reaction of 60 μM 4-NBA-CoA with 70 μM 4-CBA-CoA dehalogenase are shown. The product formation curve was analyzed with a single-exponential equation to give $k_{obs} = 7 \times 10^{-4}$ s^{-1}. The covalent enzyme was not detected. Similarly, aliquots removed from the reaction mixtures of 4-FBA-CoA and 4-CBA-CoA dehalogenase did not contain detectable levels of EAr. These results demonstrate that the reaction intermediate EAr does not accumulate to a significant extent during dehalogenase-catalyzed hydrolyses of 4-FBA-CoA and 4-NBA-CoA. Thus, EAr will not contribute significantly to the Raman spectra measured for mixtures of dehalogenase and 4-FBA-CoA or 4-NBA-CoA.

Stopped-Flow Absorption Studies of the Single-Turnover Reaction of 4-NBA-CoA. In the introduction, we speculated that in the dehalogenase-catalyzed reactions of 4-FBA-CoA and 4-NBA-CoA the EMc might accumulate to a level ~10% of the total enzyme present. This estimate is based on a slow rate of fluoride or nitrite expulsion from EMc and on the assumption that the rates of the forward (200 s^{-1}) and reverse (2000 s^{-1}) directions of the E·S to EMc step are the same in the 4-FBA-CoA and 4-NBA-CoA reactions as they are in the 4-CBA-CoA reaction. Here, the progress of a single-turnover reaction of dehalogenase (70 μM) and 4-NBA-CoA (60 μM) was monitored using stopped-flow absorption techniques. The absorption curves measured at 430 and 375 nm (Figure 6) were fitted using the kinetic model of the 4-CBA-CoA reaction but substituting the experimental values of 4-NBA-CoA k_{on} and k_{off} for k_1 and k_{-1}, and the k_{obs} for E·P formation for k_3.

The UV/visible absorption spectra of 4-NBA-CoA and 4-HBA-CoA in buffer and the UV/visible absorption difference spectra of the dehalogenase−4-NBA-CoA complex and the dehalogenase−4-HBA-CoA complex are shown in Figure 7. The UV/visible absorption difference spectra of the dehalogenase−ligand complexes were generated by subtracting the absorption spectra of the uncomplexed ligand and

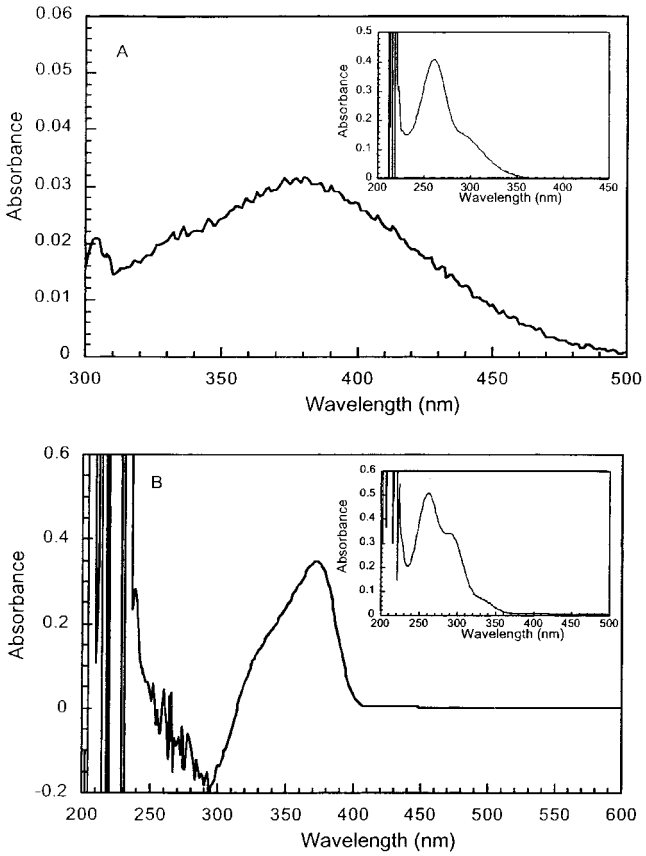

FIGURE 7: (A) UV/visible difference spectrum of the 4-CBA-CoA dehalogenase−4-NBA-CoA complex measured within 15 s after mixing equal volumes of 200 μM 4-NBA-CoA and 50 μM 4-CBA-CoA dehalogenase; and (inset) UV/visible spectrum of 25 μM 4-NBA-CoA in 50 mM K^+Hepes (pH 7.5, 25 °C) (B) UV/visible difference spectrum of the 4-CBA-CoA dehalogenase−4-HBA-CoA complex measured after mixing equal volumes of 200 μM 4-HBA-CoA and 50 μM 4-CBA-CoA dehalogenase; and (inset) UV/visible spectrum of 25 μM 4-HBA-CoA in 50 mM K^+Hepes (pH 7.5, 25 °C).

enzyme (measured with a tandem cell) from that of the enzyme−ligand complex. Thus, the difference spectrum reveals shifts in ligand absorption induced by the environment of the enzyme active site. From previous studies (*9*, *12*), it is known that the dehalogenase active site induces a large red shift in the absorption band deriving from the benzoyl chromophore of the substrate or product ligand owing to the polarization of the ring π-electron density. In the case of the 4-HBA-CoA ligand, the 260 nm adenine absorption maximum is unchanged upon enzyme complexation while the benzoyl absorption maximum is shifted from 290 to 375 nm. This shift appears in the difference spectrum as a trough at 290 nm and peak at 375 nm. The absorption spectrum of 4-NBA-CoA in buffer reveals that the 260 nm adenine absorption overlaps with a broad benzoyl absorption band extending to 350 nm. The difference spectrum (measured within 15 s after mixing and thus deriving from the dehalogenase−4-NBA-CoA complex in equilibrium with the EMc complex) indicates significant absorption out to 500 nm, well beyond the absorption range of solvated 4-NBA-CoA or the dehalogenase−4-HBA-CoA complex. This long-wavelength absorption occurs because of the resonance of the nitro substituent with the benzoyl ring, coupled with the polarization of the ring by the enzyme active site.

The binding reaction between 4-NBA-CoA and the dehalogenase can be monitored at 430 nm where the dehalogenase−4-NBA-CoA complex absorbs since no other species is expected to contribute at this wavelength. The EMc complex is not expected to absorb at 430 nm wavelength because the nitro substituent, which contributes to the long-wavelength absorption of the benzoyl moiety of the substrate through resonance, does not contribute to the ring π-electron density of the σ-complex. Likewise, the absorption by the enzyme−product complex does not extend out to 430 nm.

The 0−200 ms 430 nm absorption curve shown in Figure 6A was fitted with KINSIM (*31*) using a kinetic model consisting of the substrate binding and EMc forming steps:

$$E + S \underset{k_{-1}}{\overset{k_1}{\rightleftharpoons}} E{\cdot}S \underset{k_{-2}}{\overset{k_2}{\rightleftharpoons}} EMc$$

where $k_1 = 2.8\ s^{-1}\ \mu M^{-1}$, $k_{-1} = 1.0\ s^{-1}$, $k_2 = 200\ s^{-1}$, and $k_{-2} = 1000\ s^{-1}$; and at 430 nm, E·S $\epsilon = 0.92\ mM^{-1}\ cm^{-1}$, and for the E, S, and EMc $\epsilon = 0.0\ mM^{-1}\ cm^{-1}$. Like the dehalogenase−product complex, the dehalogenase−4-NBA-CoA complex absorbs at 375 nm. The 0−200 ms 375 nm absorption curve shown in Figure 6A derives from the formation of the dehalogenase−4-NBA-CoA complex, however, and not from the formation of the enzyme−product complex which occurs at longer reaction times (see below). The 375 nm absorption curve was fitted to the kinetic model shown above, using E·S $\epsilon = 1.23\ mM^{-1}\ cm^{-1}$, and the same rate constants used to fit the 430 nm absorption curve.

At longer reaction periods (0−3600 s), the absorption at 430 nm begins to decrease and the absorption at 375 nm to increase from the respective plateaus reached at the attainment of the quasi-equilibrium between the 4-NBA-CoA, dehalogenase, dehalogenase−4-NBA-CoA complex, and the EMc. The 0−3600 s 430 and 375 nm absorption curves shown in Figure 6B were fitted with KINSIM (*31*) using a kinetic model consisting of all of the reaction steps:

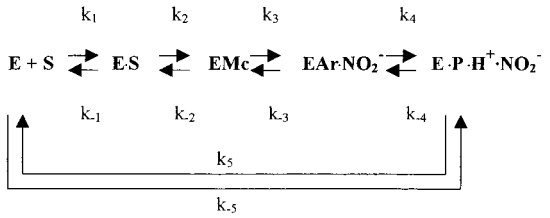

where $k_1 = 2.8\ s^{-1}\ \mu M^{-1}$, $k_{-1} = 1.0\ s^{-1}$, $k_2 = 200\ s^{-1}$, $k_{-2} = 1000\ s^{-1}$, $k_3 = 0.005\ s^{-1}$, $k_{-3} = 0\ s^{-1}$, $k_4 = 25\ s^{-1}$, $k_{-4} = 0\ s^{-1}$, $k_5 = 1\ s^{-1}$, $k_{-5} = 8\ \mu M^{-1}\ s^{-1}$, E·S $\epsilon = 1.23\ mM^{-1}\ cm^{-1}$ at 375 nm, E·P $\epsilon = 10.5\ mM^{-1}\ cm^{-1}$ at 375 nm, and E·S $\epsilon = 0.92\ mM^{-1}\ cm^{-1}$ at 430 nm.

The goodness of fit of the simulated curves generated by using the original kinetic model derived for the dehalogenase−4-CBA-CoA reaction (*5*) with adjustments made for the substrate binding rate constants (experimental k_{on} and k_{off} values for 4-NBA-CoA substituted) and the EMc to EAr rate constant (to reflect the lower mobility of the nitrite leaving group) supports our original hypothesis that the lifetime of the EMc intermediate can be increased by substituting the 4-CBA-CoA with 4-NBA-CoA as substrates. The simulated values for $k_2 = 200\ s^{-1}$ and $k_{-2} = 1000\ s^{-1}$ reflect the accumulation of EMc derived from 4-NBA-CoA to 20% of the enzyme present. Realistically, the stopped-

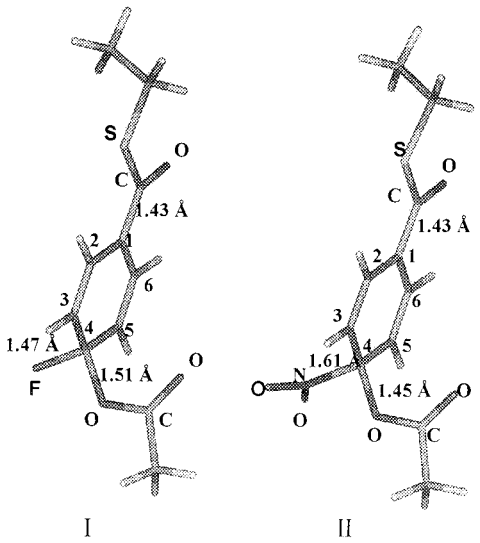

FIGURE 8: Meisenheimer compounds I and II predicted by quantum mechanical analysis. The ring bond lengths in I are C1C2═C1C6 = 1.43 Å; C2C3═C5C6 = 1.37 Å; C3C4═C4C5 = 1.46 Å. The ring bond lengths in II are C1C2═C1C6 = 1.42 Å; C2C3═C5C6 = 1.35 Å; C3C4═C4C5 = 1.47 Å.

flow data cannot be used to define these two rate constants with precision. Nevertheless, the fit is exquisitely sensitive to the ratio k_2/k_{-2} and to the value of k_3 used as input. Only by increasing the value of k_3 can the ratio of k_2/k_{-2} be reduced and the goodness of fit preserved. Thus, 20% may be a reasonable estimate of the fraction of enzyme which accumulates as EMc during the course of the Raman spectral experiments described below.

Raman Spectral Analysis of Dehalogenase Reaction Mixtures of 4-FBA-CoA and 4-NBA-CoA

Density Functional Theory Calculations on the Mc. Figure 8 illustrates the structural features of the predicted Meisenheimer compounds obtained by using the ab initio HF method [HF/6-31+G(d)]. Noticeably, the ring C4−F bond is elongated from 1.36 Å in the substrate 4-FBA-CoA to 1.47 Å in the Meisenheimer compound I, and that of the ring C4-nitro N bond is elongated from 1.46 Å in the substrate 4-NBA-CoA to 1.61 Å in compound II. While the ring remains planar, it possesses evident double bond/single bond character, with sp^2 hybridization at the C1, C2, C3, C5, and C6 atoms, and sp^3 hybridization at the C4 atom, indicating the absence of full electron density delocalization in the related five sp^2-cabon atoms. The exocyclic C1−C(═O) bond is shortened from 1.50 Å in the substrates to 1.43 Å in the Mc compounds, demonstrating charge delocalization to the thioester group, and, hence, small yet effective activation of the ring under the carboxylate's attack, through resonance stabilization. It is expected that in the enzyme environment the stabilizing effect of the CoA thioester group on the Mc compounds can be further enhanced by the thioester's participation in a network of peptide hydrogen bonds (*6, 27*) that starts from the Phe64 and Gly114 backbone N−H (Figures 1 and 2). Further minimal energy calculations by the density functional theory (DFT) method [B3LYP/6-31+G(d)] yielded an optimized geometry for Meisenheimer compound I quite similar to that seen for compound I in Figure 8. These calculations also yielded a vibrational structure without a negative vibrational frequency, further indicating that the structure represents a truly stable intermediate on the reaction pathway. The DFT frequencies of Meisenheimer compound I are listed in Table 2. The raw frequencies were converted by a single scaling factor of 0.975, mainly to correct for the anharmonicity effect and the use of finite basis set, according to a previous evaluation work (*36*).

Table 2: DFT Predicted Frequencies (cm^{-1}) of Meisenheimer Compound I[a]

mode no.	frequency	Raman activity	normal mode[b]
66	1740.0	4	acetoxy ester C═O stretch
65	1644.3	179	thioester C═O stretch + 8a-like C═C symmetric stretch
64	1595.0	118	8a-like C═C symmetric stretch + thioester C═O stretch
63	1524.9	56	two C═C antisymmetric stretch
59	1459.4	23	8b-like ring quadrant stretch
57	1447.7	18	19a-like ring stretch
53	1304.2	34	19b-like ring stretch
51	1277.5	17	3-like ring stretch
49	1258.3	14	7a′-like ring bend + C1−C stretch + ring C−H i.p. bend + acetoxy ester −O−C═O bend
48	1245.6	5	acetoxy ester −O−C═O bend + 7a′-like ring i.p. bend + C−H i.p. bend
47	1176.4	14	9a-like ring C−H i.p. bend
46	1101.2	1	15-like ring C−H i.p. bend
41	983.5	3	18a-like ring i.p. bend
40	960.9	10	ethyl C−C stretch
39	946.9	3	ring C−H o.o.p. bend
38	939.3	9	C−O−C bend + 18a
37	920.5	2	ring C−H o.o.p. bend
36	909.0	27	13-like ring i.p. bend
35	847.4	7	1-like ring bend + C−S stretch
34	797.4	1	ring o.o.p. bend
33	734.7	4	ring C−H o.o.p. bend
31	724.7	13	ring i.p. bend
30	718.3	15	ring C−H o.o.p. bend
29	662.2	27	S−C stretch
28	653.4	15	acetoxy ester O−C−C bend + ring i.p. bend + C−F stretch
27	628.8	5	C−H o.o.p. bend
26	610.5	9	6b-like i.p. bend
25	590.9	1	acetoxy ester C═O o.o.p. bend
24	573.1	4	18b-like ring i.p. bend + C−F stretch
23	537.9	2	ring o.o.p. bend
22	504.4	3	ring o.o.p. bend

[a] A total of 78 normal modes exist for Meisenheimer compound I. Normal modes associated only with the *S*-ethyl group and the methyl group from the acetoxy ester are mainly composed of C−H deformation and/or C−C stretching and therefore not listed here. [b] Wilson notations for benzenoid ring modes can roughly be adopted here to describe the ring modes of the Meisenheimer compound. i.p., in-plane; o.o.p., out-of-plane.

Detection of EMc by Raman Spectroscopy. Detection of the EMc by Raman spectroscopy proved successful. Previous studies of the wild-type and mutant dehalogenase complexes with substrate, substrate analogues, and product have culminated in a large database for the assignments of peaks positions associated with thioester C═O and benzoyl ring C−H bond motions of the ligands in solution and in the polarizing environment of the dehalogenase active site (*7, 8, 12, 37*). Now we analyze the Raman spectra of 4-FBA-CoA and 4-NBA-CoA complexed with wild-type and H90Q

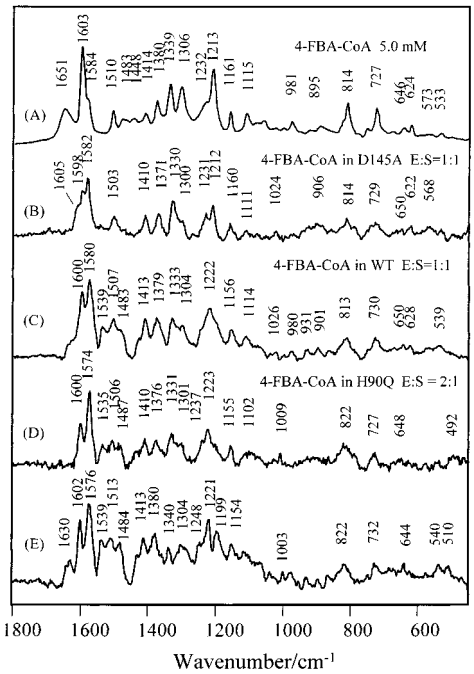

FIGURE 9: Raman spectra of 4-FBA-CoA in various states. (A) Free 4-FBA-CoA, 5.0 mM, in 50 mM Tris-HCl buffer; (B) 4-FBA-CoA bound to D145A (272 μM), 1:1 ratio; (C) bound to WT (350 μM), E:S = 1:1 ratio; (D) bound to H90Q (260 μM), E:S = 2:1; (E) a double difference Raman spectrum (C minus B) that is dominated by modes from the Meisenheimer complex. All solutions were made at pH 7.5, Tris buffer, 50 mM.

dehalogenase in the context of the spectra obtained for these ligands bound to D145A dehalogenase—in which EMc formation cannot occur.

Raman difference spectra of 4-FBA-CoA in solution, bound to wild-type and H90Q dehalogenase, and bound to D145A dehalogenase, are shown in Figure 9. The key Raman modes found in the spectrum of the solvated 4-FBA-CoA are the C═O stretch at 1651 cm^{-1} and the phenyl ring modes at 1603, 1584, and 1213 cm^{-1}. The feature near 1232 cm^{-1} is a 7a type ring mode containing a contribution from a C−F stretching motion (Table S1 in Supporting Information lists detailed assignments for vibrational modes of 4-FBA-CoA). Upon binding to wild-type or H90Q enzyme, the C═O is strongly polarized, resulting in a shift from 1651 cm^{-1} to a shoulder near 1605 cm^{-1}. The ring modes at ca. 1600 cm^{-1} are only slightly perturbed, showing small changes in frequencies and relative intensities (although this region does contain some contribution from the Mc; see below). Similar effects are seen in the Raman difference spectrum of 4-methylbenzoyl-CoA bound to the dehalogenase active site (*8*, *12*). However, the spectrum of WT dehalogenase-bound 4-FBA-CoA reveals novel features not seen for bound 4-methylbenzoyl-CoA. Specifically, the 4-FBA-CoA complex gives rise to unique features in the form of fairly broad bands near 1222 and between 1480 and 1540 cm^{-1}. Similar broad features are seen for 4-FBA-CoA binding to the H90Q form of dehalogenase. Crucially, however, these "novel" bands are absent for 4-FBA-CoA bound to the D145A mutant enzyme, which cannot form an EMc. We assign the "novel" broad bands from the 4-FBA-CoA complexes with WT and H90Q enzymes to modes from the EMc. The "novel" bands persist over time, consistent with the slow conversion rate of the EMc revealed by the kinetic study. Strong supporting evidence comes from the quantum mechanical calculations and from parallel studies with 4-NBA-CoA−dehalogenase complexes.

Table 2 lists the predicted Raman frequencies for the Mc based on the DFT calculations. The calculations were undertaken for the negatively charged Mc analogue compound I in vacuo, and thus an exact correspondence between the calculated values and those for the Mc in the active site is not expected. However, the calculations do provide good insight into the expected distribution of normal modes. In Table 2, modes 63 and 59 are medium intensity Raman features, associated with ring stretches, and these can account for the broad intensity between 1480 and 1540 cm^{-1} seen in Figure 9C,D. The increase in intensity and apparent band broadening near 1300 cm^{-1} in Figure 9C,D upon forming the enzyme complex is explained by the presence of the 19b-like ring stretch for the Mc, mode 53 in Table 2. Some or all of the Mc modes 51, 49, 48 explain the appearance of the broad feature around 1222 cm^{-1} in Figure 9. Thus, the calculations on the Mc provide a one-to-one correspondence between the most active Raman modes predicted for the Mc between 1100 and 1550 cm^{-1} and the observed intensity increases for the complex in Figure 9. In addition, the calculations predict that the 1590−1650 cm^{-1} region will contain significant contributions from Mc ring modes which will overlap with those from the E·S complex. This is borne out by the "double difference" spectrum seen in Figure 9E. These data were obtained by subtracting Figure 9B from Figure 9C, and the most intense Mc modes are indeed in the 1600 cm^{-1} region. As a result of the multiple data subtractions leading to Figure 9E, minor peaks have to be treated with caution, and the appearance of modes due to protein also is a possibility if conformational change accompanies Mc formation. However, Figure 9E suggests that the Mc has quite a rich Raman spectrum and some of the broad peaks we have commented on are due to multiple features.

Raman difference spectra of 4-NBA-CoA in solution, bound to WT and H90Q dehalogenase, and bound to D145A dehalogenase are compared in Figure 10. In the figure the NO_2 group contributes intensity at 1359 cm^{-1} (NO_2 symmetric stretch) and 1113 cm^{-1} (N−C stretch) (see detailed assignments for 4-NBA-CoA in Table S2 of Supporting Information). As in the case of the complexes involving 4-FBA-CoA (Figure 9), the key observations are the presence of broad features near 1530 and 1220 cm^{-1} for 4-NBA-CoA binding to wild-type and H90Q enzymes (Figure 10C,D) and their absence in the spectrum from the complex with D145A enzyme (Figure 10B). Again, the broad features are assigned to modes from the EMc.

The 4-nitro group is a better leaving group than 4-F, and the 4-NBA-CoA dehalogenase (WT) turns over to the product complex 4-HBA-CoA−dehalogenase at a rate of 7×10^{-4} s^{-1}. Figure 11 follows this reaction via the Raman difference spectrum, from 1 to 79 min after mixing. At 56 min, the Raman peaks of the substrate at 1586 cm^{-1} (phenyl ring mode) and 1358 cm^{-1} ($-NO_2$, symmetric stretch) have almost disappeared to be replaced by the characteristic modes of the bound product at 1561 and 1523 cm^{-1} as reported previously for the latter complex (*7*, *8*, *12*). By fitting the change in intensity of the 1587 cm^{-1} band with time, we obtained a single-exponential decay with a rate of 5.4×10^{-4}

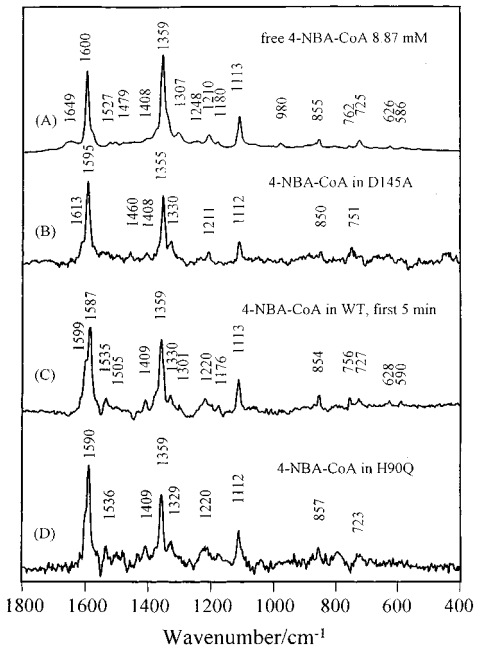

FIGURE 10: Raman spectra of 4-NBA-CoA in various states. (A) Free 4-NBA-CoA, 8.87 mM, in Tris-HCl buffer, 50 mM; (B) 4-NBA-CoA bound to D145A (233 μM); (C) bound to WT (253 μM), averaged data for the first 5 min reaction; (D) bound to H90Q (221 μM). All solutions were made at pH 7.5, 50 mM Tris-HCl buffer. Enzyme:ligand ratios for all complexes were 1:1.

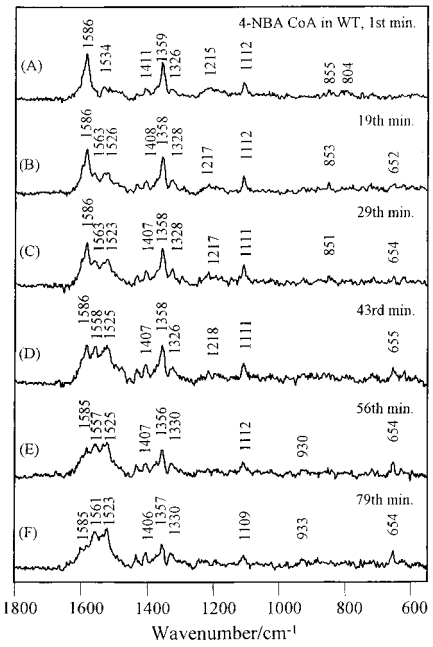

FIGURE 11: Time-dependent Raman spectra of 4-NBA-CoA bound to 253 μM WT dehalogenase (A) at reaction $t = 1$ min, (B) at $t =$ 19th min, (C) at $t = 29$th min, (D) at $t = 43$rd min, (E) at $t = 56$th min, (F) at $t = 79$th min. The solutions were made at pH 7.5, Tris buffer, 50 mM. Enzyme:ligand ratio = 1:1.

s^{-1}, in good agreement with the value determined from the kinetic studies. The critical observation in Figure 11 is that the broad band near 1215 cm^{-1} (see 1 min trace) appears to track the disappearance of the substrate bands at 1586 and 1358 cm^{-1} in the E·S complex. This discussion cannot be extended to the "novel" broad band near 1500 cm^{-1} due to interference from the product bands. Since the 1215 cm^{-1} band is absent in the substrate and the product, it must be due to intermediate, and its intensity diminution tracking that of bound substrate strongly supports the concept that we are seeing an equilibrium population of E·S ⇔ EMc.

We do not know the absolute Raman intensities (scattering cross sections) associated with the EMc. However, the appearance of novel weak-to-medium intensity bands near 1220 and 1530 cm^{-1} is consistent with a minor population of EMc. In the E·S and EMc band overlapped region (1600−1570 cm^{-1}), the increase in the relative intensity of the 1580 cm^{-1} band for the 4-FBA-CoA complex relative to the CoA adenine band near 1330 cm^{-1} (Figure 9) is about 30% in the WT complex compared to the D145A complex. Again, this is consistent with an EMc population in the ∼20−30% range. A similar increase by 30% in the intensity for the band near 1590 cm^{-1} in the WT vs D145A enzyme occurs for 4-NBA-CoA binding (Figure 10), when using the corresponding CoA band at 1330 cm^{-1} as a reference.

Summary. Detailed kinetic studies on 4-FBA-CoA or 4-NBA-CoA reacting with dehalogenase are consistent with an equilibrium population of Michaelis and Meisenheimer complexes remaining in reaction mixtures for tens of minutes or longer. For these reaction mixtures, two regions in their Raman difference spectra show "novel" features that are assigned to a population of EMc. The assignment is supported by high level quantum mechanical calculations. This is one of the first reports of the use of Raman spectroscopy to detect transient intermediates in a complex reaction scheme and illustrates the power of a tripartite kinetic, theoretical, and spectroscopic approach.

ACKNOWLEDGMENT

The computer time on the SV1 parallel vector processor at Ohio Supercomputer Center is gratefully acknowledged.

SUPPORTING INFORMATION AVAILABLE

Table S1, DFT predicted frequencies (cm^{-1}) of 4-FBA-CoA model compound *S*-ethyl 4-fluorobenzoate thioester between 2000 and 400 cm^{-1}; Table S2, DFT predicted frequencies (cm^{-1}) of 4-NBA-CoA model compound *S*-ethyl 4-nitrobenzoate thioester between 2000 and 400 cm^{-1}; and Table S3, complete list of DFT predicted frequencies (cm^{-1}) of Meisenheimer compound I between 2000 and 400 cm^{-1}. This information is available free of charge via the Internet at http://pubs.acs.org.

REFERENCES

1. Scholten, J. D., Chang, K. H., Babbitt, P. C., Charest, H., Sylvestre, M., and Dunaway-Mariano, D. (1991) *Science 253*, 182−185.
2. Crooks, G. P., and Copley, S. D. (1994) *Biochemistry 33*, 11645−11649.
3. Loffler, F., Lingens, F., and Muller, R. (1995) *Biodegradation 6*, 203−212.
4. Dunaway-Mariano, D., and Babbitt, P. C. (1994) *Biodegradation 5*, 259−276.
5. Zhang, W., Wei, Y., Luo, L., Taylor, K. L., Yang, G., Dunaway-Mariano, D., Benning, M. M., and Holden, H. M. (2001) *Biochemistry 40*, 13474−13482.
6. Luo, L., Taylor, K. L., Xiang, H., Wei, Y., Zhang, W., and Dunaway-Mariano, D. (2001) *Biochemistry 40*, 15684−15692.
7. Dong, J., Xiang, H., Luo, L., Dunaway-Mariano, D., and Carey, P. R. (1999) *Biochemistry 38*, 4198−4206.
8. Clarkson, J., Tonge, P. J., Taylor, K. L., Dunaway-Mariano, D., and Carey, P. R. (1997) *Biochemistry 36*, 10192−10199.
9. Taylor, K. L., Xiang, H., Liu, R. Q., Yang, G., and Dunaway-Mariano, D. (1997) *Biochemistry 36*, 1349−1361.

10. Benning, M. M., Taylor, K. L., Liu, R. Q., Yang, G., Xiang, H., Wesenberg, G., Dunaway-Mariano, D., and Holden, H. M. (1996) *Biochemistry 35*, 8103−8109.
11. Liu, R. Q., Liang, P. H., Scholten, J. D., and Dunaway-Mariano, D. (1995) *J. Am. Chem. Soc. 117*, 5003−5004.
12. Taylor, K. L., Liu, R. Q., Liang, P. H., Price, J., Dunaway-Mariano, D., Tonge, P. J., Clarkson, J., and Carey, P. R. (1995) *Biochemistry 34*, 13881−13888.
13. Crooks, G. P., Xu, L., Barkley, R. M., and Copley, S. D. (1995) *J. Am. Chem. Soc. 117*, 10791−10798.
14. Yang, G., Liang, P. H., and Dunaway-Mariano, D. (1994) *Biochemistry 33*, 8527−8531.
15. Liang, P. H., Yang, G., and Dunaway-Mariano, D. (1993) *Biochemistry 32*, 12245−12250.
16. Zheng, Y. J., and Bruice, T. C. (1997) *J. Am. Chem. Soc. 119*, 3868−3877.
17. Bruice, T. C., and Lightstone, F. C. (1999) *Acc. Chem. Res. 32*, 127−136.
18. Yang, G., Liu, R. Q., Taylor, K. L., Xiang, H., Price, J., and Dunaway-Mariano, D. (1996) *Biochemistry 35*, 10879−10885.
19. Miller, J. (1968) in *Reaction Mechanisms in Organic Chemistry* (Earborn, C., and Chapman, N. B., Eds.) Vol. 8, pp 137−179, Elsevier, New York.
20. Terrier, F. (1982) *Chem. Rev. 82*, 78−150.
21. Lenke, H., and Knackmuss, H.-J. (1992) *Appl. Environ. Microbiol. 58*, 2598−2606.
22. Rieger, P.-G., Sinnwell, V., Preub, A., Francke, W., and Knackmuss, H.-J. (1999) *J. Bacteriol. 181*, 1189−1195.
23. Graminski, G. F., Zhang, P., Sesay, M. A., Ammon, H. L., and Armstrong, R. N. (1989) *Biochemistry 28*, 6252−6258.
24. Liou, J.-Y., Huang T.-M., and Chang, G.-G. (2000) *J. Protein Chem. 19*, 615−620.
25. Ji, X., Armstrong, R. N., and Gilliland, G. L. (1993) *Biochemistry 32*, 12949−12954.
26. Prade, L., Huber, R., Manoharan, T. H., Fahl, W. E., and Reuter, W. (1997) *Structure 5*, 1287−1295.
27. Guo, H., and Salahub, D. R. (1998) *Angew. Chem., Int. Ed. Engl. 37*, 2985−2990.
28. Mieyal, J. J., Webster, L. T., Jr., and Siddiqui, U. A. (1974) *J. Biol. Chem. 249*, 2633−2640.
29. Bradford, M. (1976) *Anal. Biochem. 72*, 248−254.
30. Anderson, K. S., Sikorski, J. A., and Johnson, K. A. (1988) *Biochemistry 27*, 7395−7406.
31. Barshop, B. A., Wrenn, R. F., and Frieden, C. (1983) *Anal. Biochem.130*, 134−145.
32. Frisch, M. J., Trucks, G. W., Schlegel, H. B., Scuseria, G. E., Robb, M. A., Cheeseman, J. R., Zakrzewski, V. G., Montgomery, J. A., Stratmann, R. E., Burant, J. C., Dapprich, S., Millam, J. M., Daniels, A. D., Kudin, K. N., Strain, M. C., Farkas, O., Tomasi, J., Barone, V., Cossi, M., Cammi, R., Mennucci, B., Pomelli, C., Adamo, C., Clifford, S., Ochterski, J., Petersson, G. A., Ayala, P. Y., Cui, Q., Morokuma, K., Malick, D. K., Rabuck, A. D., Raghavachari, K., Foresman, J. B., Cioslowski, J., Ortiz, J. V., Stefanov, B. B., Liu, G., Liashenko, A., Piskorz, P., Komaromi, I., Gomperts, R., Martin, R. L., Fox, D. J., Keith, T., Al-Laham, M. A., Peng, C. Y., Nanayakkara, A., Gonzalez, C., Challacombe, M., Gill, P. M. W., Johnson, B., Chen, W., Wong, M. W., Andres, J. L., Gonzalez, C., Head-Gordon, M., Replogle, E. S., and Pople, J. A. (1998) *Gaussian 98 A.9*, Gaussian, Inc., Pittsburgh, PA.
33. Becke, A. D. (1993) *J. Chem. Phys. 98*, 5684−5652.
34. Lee, C., Yang, W., and Parr, R. G. *(1988) Phys. Rev. B 37*, 785−789.
35. Persson, J., Axelsson, S., and Matsson, O. (1996) *J. Am. Chem. Soc. 118*, 20−23.
36. Scott, A. P., and Radom, L. (1996) *J. Phys. Chem. 100*, 16502−16513.
37. Xiang, H, Dong, J., Carey, P. R., and Dunaway-Mariano, D. (1999) *Biochemistry 38*, 4207−4213.

BI020186+